Preprints of the 19th World Congress
The International Federation of Automatic Control
Cape Town, South Africa. August 24-29, 2014

Adaptive control for UAVs equipped with a robotic arm

F. Caccavale , G. Giglio , G. Muscio , F. Pierri .

School of Engineering, University of Basilicata, 85100 Potenza, Italy
{fabrizio.caccavale, gerardo.giglio, giuseppe.muscio, francesco.pierri}@unibas.it

Abstract: This paper deals with the trajectory tracking control for quadrotor aerial vehicles equipped with a robotic manipulator. The proposed approach is based on a two-layer controller: in the top layer, an inverse kinematics algorithm computes the motion references for the actuated variables while in the bottom layer, an adaptive motion control algorithm is in charge of tracking the motion references. A stability analysis of the closed-loop system is developed. Finally, a simulation case study is presented to prove the effectiveness of the approach.

Keywords: Robotics; Autonomous Vehicles; Adaptive Control.

1. INTRODUCTION

Unmanned Aerial Vehicles (UAVs) are employed in a large number of applications, such as surveillance of indoor or outdoor environments, remote inspection and monitoring of hostile environments. There exist numerous types of UAVs, but in the last years, the quadrotor helicopters are emerging as popular platform, due to their simple structure, the larger payload capability an the higher manoeuvrability with respect to the single-rotor vehicles.

Motion control of a quadrotor vehicle is a challenging issue, since the quadrotor is an under-actuated system, with two directions not directly actuated. Both linear, such as PID controllers (Hoffmann et al., 2007), and nonlinear controllers, such as model predictive control (Kim and Shim, 2003), backstepping and sliding mode techniques (Bouabdallah and Siegwart, 2005), have been proposed in the last decade. In particular, very interesting is the hierarchical approach, based on an inner-outer loop, in Kendoul et al. (2008) that exploit the conceptual separation between position and orientation of a quadrotor. Some adaptive control laws have been proposed: in Palunko and Fierro (2011) the mathematical model of the UAV system is rewritten in such a way to point out its linear dependency to the center of gravity position, which is then used in a feedback linearization approach; in Antonelli et al. (2013) the effect of constant exogenous forces and moments and the presence of unknown dynamic parameters (e.g., the position of the center of mass) have been considered.

Recently, UAVs have been employed in tasks as grasping and manipulation (Spica et al., 2012) as well as in cooperative transportation (Maza et al., 2010). These are challenging issues since the vehicle is characterized by an unstable dynamics and the presence of the object causes nontrivial coupling effects (Pounds et al., 2011). UAVs equipped with a robotic arm for aerial manipulation tasks have been proposed in Lippiello and Ruggiero (2012), where the dynamic model of the whole system, UAV plus manipulator, is devised and a Cartesian impedance control is developed in such a way to cope with contact forces and external disturbances, and in Kondak et al. (2013), where the influences imposed on an helicopter from a manipulator are analyzed.

In Arleo et al. (2013) the problem of motion control of the end-effector of a robot manipulator mounted on a quadrotor helicopter is tackled through a hierarchical control architecture. Namely, in the top layer, an inverse kinematics algorithm computes the motion references for the actuated variables, i.e., position and yaw angle of the quadrotor vehicle and joint variables for the manipulator, while in the bottom layer, a motion control algorithm is in charge of tracking the motion references. In this paper, the previous scheme is extended by adding, at the motion control level, an adaptive term, in charge of taking into account modeling uncertainties and overcoming some assumptions done in Arleo et al. (2013) due to the underactuation of the system. Moreover, a rigorous stability analysis of the closed-loop system is performed. Finally, in order to demonstrate the effectiveness of the approach, a simulation case study is developed.

2. MODELING

Let us consider a system composed by a quadrotor vehicle equipped with a n-DOF robotic arm, depicted in Fig. 1.

2.1 Kinematics

Let Σ_b denotes the vehicle body-fixed reference frame with origin at the vehicle center of mass; its position with respect to the world fixed inertial reference frame, Σ, is given by the (3×1) vector $\boldsymbol{p}_b$, while its orientation is given by the rotation matrix $\boldsymbol{R}_b$

$$\boldsymbol{R}_b(\boldsymbol{\phi}_b)=\begin{bmatrix} c_\psi c_\theta & c_\psi s_\theta s_\varphi - s_\psi c_\varphi & c_\psi s_\theta c_\varphi + s_\psi s_\varphi \\ s_\psi c_\theta & s_\psi s_\theta s_\varphi + c_\psi c_\varphi & s_\psi s_\theta c_\varphi - c_\psi s_\varphi \\ -s_\theta & c_\theta s_\varphi & c_\theta c_\varphi \end{bmatrix}, \quad (1)$$

where $\boldsymbol{\phi}_b = [\psi\ \theta\ \varphi]^T$ is the triple of ZYX yaw-pitch-roll angles and c_γ and s_γ denote, respectively, $\cos\gamma$ and $\sin\gamma$.

⋆ The research leading to these results has received funding from the European Community's Seventh Framework Programme under grant agreement n. 287617 (collaborative project ARCAS).

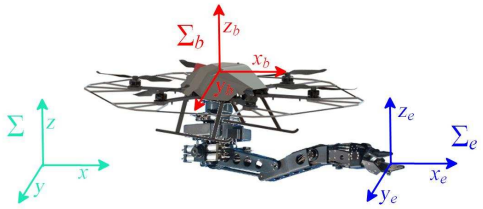

Fig. 1. Quadrotor and robotic arm system with the corresponding frames.

Let us consider the frame Σ_e attached to the end effector of the manipulator (see Fig. 1). The position and the orientation of Σ_e with respect to Σ are given by

$$\boldsymbol{p}_e = \boldsymbol{p}_b + \boldsymbol{R}_b \boldsymbol{p}_{eb}^b \,, \tag{2}$$

$$\boldsymbol{R}_e = \boldsymbol{R}_b \boldsymbol{R}_e^b \,, \tag{3}$$

where the vector $\boldsymbol{p}_{eb}^b$ and the matrix $\boldsymbol{R}_e^b$ describe the position and the orientation of Σ_e with respect to Σ_b, respectively. The linear and angular velocities $\dot{\boldsymbol{p}}_e$ and $\boldsymbol{\omega}_e$ of Σ_e in the fixed frame are obtained by differentiating (2)-(3)

$$\dot{\boldsymbol{p}}_e = \dot{\boldsymbol{p}}_b - \boldsymbol{S}(\boldsymbol{R}_b \boldsymbol{p}_{eb}^b)\boldsymbol{\omega}_b + \boldsymbol{R}_b \dot{\boldsymbol{p}}_{eb}^b \,, \tag{4}$$

$$\boldsymbol{\omega}_e = \boldsymbol{\omega}_b + \boldsymbol{R}_b \boldsymbol{\omega}_{eb}^b \,, \tag{5}$$

where $\boldsymbol{S}(\cdot)$ is the (3×3) skew-symmetric matrix operator performing the cross product (Siciliano et al., 2009), and $\boldsymbol{\omega}_{eb}^b = \boldsymbol{R}_b^{\mathrm{T}} (\boldsymbol{\omega}_e - \boldsymbol{\omega}_b)$ is the relative angular velocity between the end effector and the frame Σ_b, expressed in Σ_b.

Let $\boldsymbol{q}$ be the $(n \times 1)$ vector of joint coordinates of the manipulator. Then, $\boldsymbol{p}_{eb}^b(\boldsymbol{q})$ and $\boldsymbol{R}_e^b(\boldsymbol{q})$ represent the usual direct kinematics equations of a ground-fixed manipulator with respect to its base frame, Σ_b. The (6×1) vector of the generalized velocity of the end-effector with respect to Σ_b, $\boldsymbol{v}_{eb}^b = \left[\dot{\boldsymbol{p}}_{eb}^{b\mathrm{T}} \; \boldsymbol{\omega}_{eb}^{b\mathrm{T}}\right]^{\mathrm{T}}$, can be expressed in terms of the joint velocities $\dot{\boldsymbol{q}}$ via the manipulator Jacobian $\boldsymbol{J}_{eb}^b$, i.e.,

$$\boldsymbol{v}_{eb}^b = \boldsymbol{J}_{eb}^b(\boldsymbol{q})\dot{\boldsymbol{q}}. \tag{6}$$

On the basis of (4), (5) and (6), the generalized end-effector velocity, $\boldsymbol{v}_e = \left[\dot{\boldsymbol{p}}_e^{\mathrm{T}} \; \boldsymbol{\omega}_e^{\mathrm{T}}\right]^{\mathrm{T}}$, can be expressed as

$$\boldsymbol{v}_e = \boldsymbol{J}_b(\boldsymbol{q}, \boldsymbol{\phi}_b)\boldsymbol{T}_A(\boldsymbol{\phi}_b)\dot{\boldsymbol{x}}_b + \boldsymbol{J}_{eb}(\boldsymbol{q}, \boldsymbol{R}_b)\dot{\boldsymbol{q}} \,, \tag{7}$$

where $\boldsymbol{x}_b = \left[\boldsymbol{p}_b{}^{\mathrm{T}} \; \boldsymbol{\phi}_b{}^{\mathrm{T}}\right]^{\mathrm{T}}$ and

$$\boldsymbol{T}_A(\boldsymbol{\phi}_b) = \begin{bmatrix} \boldsymbol{I}_3 & \boldsymbol{O}_3 \\ \boldsymbol{O}_3 & \boldsymbol{T}(\boldsymbol{\phi}_b) \end{bmatrix}, \quad \boldsymbol{T}(\boldsymbol{\phi}_b) = \begin{bmatrix} 0 & -s_\psi & c_\psi c_\theta \\ 0 & c_\psi & s_\psi c_\theta \\ 1 & 0 & -s_\theta \end{bmatrix}, \tag{8}$$

$\boldsymbol{T}(\boldsymbol{\phi}_b)$ is the transformation matrix between the angular velocity $\boldsymbol{\omega}_b$ and the time derivative of the Euler angles $\dot{\boldsymbol{\phi}}_b$, namely $\boldsymbol{\omega}_b = \boldsymbol{T}(\boldsymbol{\phi}_b)\dot{\boldsymbol{\phi}}_b$. Matrices $\boldsymbol{J}_b$ and $\boldsymbol{J}_{eb}$ are given by

$$\boldsymbol{J}_b = \begin{bmatrix} \boldsymbol{I}_3 & -\boldsymbol{S}(\boldsymbol{R}_b \boldsymbol{p}_{eb}^b) \\ \boldsymbol{O}_3 & \boldsymbol{I}_3 \end{bmatrix}, \quad \boldsymbol{J}_{eb} = \begin{bmatrix} \boldsymbol{R}_b & \boldsymbol{O}_3 \\ \boldsymbol{O}_3 & \boldsymbol{R}_b \end{bmatrix} \boldsymbol{J}_{eb}^b \,,$$

where $\boldsymbol{I}_m$ and $\boldsymbol{O}_m$ denote $(m \times m)$ identity and null matrices, respectively.

Since the quadrotor is an under-actuated system, with 4 independent control inputs available against the 6 DOFs, the position and the yaw angle are usually the controlled variables, while pitch and roll angles are used as intermediate control inputs for position control. Hence, it is worth rewriting the vector $\boldsymbol{x}_b$ as follows

$$\boldsymbol{x}_b = \left[\boldsymbol{\eta}_b^{\mathrm{T}} \; \boldsymbol{\sigma}_b^{\mathrm{T}}\right]^{\mathrm{T}}, \; \boldsymbol{\eta}_b = \left[\boldsymbol{p}_b^{\mathrm{T}} \; \psi\right]^{\mathrm{T}}, \; \boldsymbol{\sigma}_b = \left[\theta \; \varphi\right]^{\mathrm{T}}.$$

Thus, the differential kinematics (7) becomes

$$\begin{aligned} \boldsymbol{v}_e &= \boldsymbol{J}_\eta(\boldsymbol{q}, \boldsymbol{\phi}_b)\dot{\boldsymbol{\eta}}_b + \boldsymbol{J}_\sigma(\boldsymbol{q}, \boldsymbol{\phi}_b)\dot{\boldsymbol{\sigma}}_b + \boldsymbol{J}_{eb}(\boldsymbol{q}, \boldsymbol{\phi}_b)\dot{\boldsymbol{q}} \\ &= \boldsymbol{J}_\zeta(\boldsymbol{\sigma}_b, \boldsymbol{\zeta})\dot{\boldsymbol{\zeta}} + \boldsymbol{J}_\sigma(\boldsymbol{\sigma}_b, \boldsymbol{\zeta})\dot{\boldsymbol{\sigma}}_b \,, \end{aligned} \tag{9}$$

where $\boldsymbol{\zeta} = \left[\boldsymbol{\eta}_b{}^{\mathrm{T}} \; \boldsymbol{q}^{\mathrm{T}}\right]^{\mathrm{T}}$ is the vector of controlled variables, $\boldsymbol{J}_\eta$ is composed by the first 4 columns of $\boldsymbol{J}_b\boldsymbol{T}_A(\boldsymbol{\phi}_b)$, $\boldsymbol{J}_\sigma$ by the last 2 columns of $\boldsymbol{J}_b\boldsymbol{T}_A(\boldsymbol{\phi}_b)$ and $\boldsymbol{J}_\zeta = [\boldsymbol{J}_\eta \; \boldsymbol{J}_{eb}]$.

2.2 Dynamics

The dynamic model of the system can be written as

$$\boldsymbol{M}(\boldsymbol{\xi})\ddot{\boldsymbol{\xi}} + \boldsymbol{C}(\boldsymbol{\xi}, \dot{\boldsymbol{\xi}})\dot{\boldsymbol{\xi}} + \boldsymbol{g}(\boldsymbol{\xi}) + \boldsymbol{d}(\boldsymbol{\xi}, \dot{\boldsymbol{\xi}}) = \boldsymbol{u} \,, \tag{10}$$

where $\boldsymbol{\xi} = [\boldsymbol{x}_b{}^{\mathrm{T}} \; \boldsymbol{q}^{\mathrm{T}}]^{\mathrm{T}} \in \mathbb{R}^{(6+n\times 1)}$, $\boldsymbol{M}$ represents the symmetric and positive definite inertia matrix of the system, $\boldsymbol{C}$ is the matrix of Coriolis and centrifugal terms, $\boldsymbol{g}$ is the vector of gravity forces, $\boldsymbol{d}$ explicitly takes into account disturbances, such as aerodynamic effects, and modeling uncertainties, and $\boldsymbol{u}$ is the vector of inputs

$$\boldsymbol{u} = \begin{bmatrix} \boldsymbol{u}_f \\ \boldsymbol{u}_\mu \\ \boldsymbol{u}_\tau \end{bmatrix} = \begin{bmatrix} \boldsymbol{R}_b(\boldsymbol{\phi}_b)\boldsymbol{f}_b^b \\ \boldsymbol{T}^{\mathrm{T}}(\boldsymbol{\phi}_b)\boldsymbol{R}_b(\boldsymbol{\phi}_b)\boldsymbol{\mu}_b^b \\ \boldsymbol{\tau} \end{bmatrix}, \tag{11}$$

where $\boldsymbol{\tau}$ is the $(n \times 1)$ vector of the manipulator joint torques, while $\boldsymbol{f}_b^b = [0 \; 0 \; f_z]^{\mathrm{T}}$ and $\boldsymbol{\mu}_b^b = [\mu_\psi \; \mu_\theta \; \mu_\varphi]^{\mathrm{T}}$ are, respectively, the forces and the torques generated by the 4 motors of the quadrotor, expressed in the frame Σ_b. Both f_z and $\boldsymbol{\mu}_b^b$ are related to the four actuation forces output by the quadrotor motors $\boldsymbol{f}$ via (Nonami et al., 2010)

$$\begin{bmatrix} f_z \\ \boldsymbol{\mu}_b^b \end{bmatrix} = \begin{bmatrix} 1 & 1 & 1 & 1 \\ 0 & l & 0 & -l \\ -l & 0 & l & 0 \\ c & -c & c & -c \end{bmatrix} \begin{bmatrix} f_1 \\ f_2 \\ f_3 \\ f_4 \end{bmatrix} = \boldsymbol{\Gamma}\boldsymbol{f} \,, \tag{12}$$

where $l > 0$ is the distance from each motor to the vehicle center of mass, $c = \gamma_d/\gamma_t$, and γ_d, γ_t are the drag and thrust coefficient, respectively.

The matrices introduced in (10) can be detailed by considering the expressions derived in Lippiello and Ruggiero (2012). The inertia matrix can be viewed as a block matrix

$$\boldsymbol{M}(\boldsymbol{\xi}) = \begin{bmatrix} \boldsymbol{M}_{pp} & \boldsymbol{M}_{p\phi} & \boldsymbol{M}_{pq} \\ \boldsymbol{M}_{p\phi}{}^{\mathrm{T}} & \boldsymbol{M}_{\phi\phi} & \boldsymbol{M}_{\phi q} \\ \boldsymbol{M}_{pq}{}^{\mathrm{T}} & \boldsymbol{M}_{\phi q}{}^{\mathrm{T}} & \boldsymbol{M}_{qq} \end{bmatrix},$$

where $\boldsymbol{M}_{pp} \in \mathbb{R}^{3\times 3}$, $\boldsymbol{M}_{p\phi} \in \mathbb{R}^{3\times 3}$, $\boldsymbol{M}_{pq} \in \mathbb{R}^{3\times n}$, $\boldsymbol{M}_{\phi\phi} \in \mathbb{R}^{3\times 3}$, $\boldsymbol{M}_{\phi q} \in \mathbb{R}^{3\times n}$ and $\boldsymbol{M}_{qq} \in \mathbb{R}^{n\times n}$.

Similarly, matrix $\boldsymbol{C}$ and vector $\boldsymbol{g}$ in (10) can be seen as

$$\boldsymbol{C}(\boldsymbol{\xi}, \dot{\boldsymbol{\xi}}) = \begin{bmatrix} \boldsymbol{C}_p \\ \boldsymbol{C}_\phi \\ \boldsymbol{C}_q \end{bmatrix}, \quad \boldsymbol{g}(\boldsymbol{\xi}) = \begin{bmatrix} \boldsymbol{g}_p \\ \boldsymbol{g}_\phi \\ \boldsymbol{g}_q \end{bmatrix},$$

with $\boldsymbol{C}_p \in \mathbb{R}^{3\times(6+n)}$, $\boldsymbol{C}_\phi \in \mathbb{R}^{3\times(6+n)}$, $\boldsymbol{C}_q \in \mathbb{R}^{n\times(6+n)}$ and $\boldsymbol{g}_p \in \mathbb{R}^3$, $\boldsymbol{g}_\phi \in \mathbb{R}^3$ and $\boldsymbol{g}_q \in \mathbb{R}^n$.

3. KINEMATIC CONTROL SCHEME

A two-layer control scheme is proposed: on the top layer, an inverse kinematics algorithm computes, based on the desired end-effector trajectory, the motion references for the quadrotor controlled variables and for the arm joints, then, in the bottom layer, a motion control is designed in such a way to track the reference trajectories output by

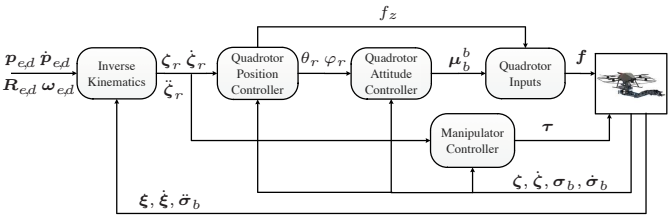

Fig. 2. Block scheme of the control architecture

the top layer (Fig. 2). In the following, it is assumed that $\dim\{\boldsymbol{\zeta}\} = n+4 \geq \dim\{\boldsymbol{v}_e\} = 6$, i.e., the number of DOFs characterizing the vehicle-manipulator system is, at least, equal to the dimension of the assigned task.

3.1 Inverse Kinematics

The time derivative of the differential kinematics (9),

$$\dot{\boldsymbol{v}}_e = \dot{\boldsymbol{J}}_\zeta(\boldsymbol{\sigma}_b,\boldsymbol{\zeta})\dot{\boldsymbol{\zeta}} + \boldsymbol{J}_\zeta(\boldsymbol{\sigma}_b,\boldsymbol{\zeta})\ddot{\boldsymbol{\zeta}} + \dot{\boldsymbol{J}}_\sigma(\boldsymbol{\sigma}_b,\boldsymbol{\zeta})\dot{\boldsymbol{\sigma}}_b + \boldsymbol{J}_\sigma(\boldsymbol{\sigma}_b,\boldsymbol{\zeta})\ddot{\boldsymbol{\sigma}}_b, \quad (13)$$

is considered to derive a second order closed-loop inverse kinematics algorithm (Caccavale et al., 1997), in charge of computing the trajectory references for the motion control loops at the bottom layer

$$\ddot{\boldsymbol{\zeta}}_r = \boldsymbol{J}_\zeta^\dagger(\boldsymbol{\sigma}_b,\boldsymbol{\zeta})\left(\dot{\boldsymbol{v}}_{e,d} + \boldsymbol{K}_v(\boldsymbol{v}_{e,d} - \boldsymbol{v}_e) + \boldsymbol{K}_p\boldsymbol{e}\right) - \boldsymbol{J}_\zeta^\dagger(\boldsymbol{\sigma}_b,\boldsymbol{\zeta})\left(\dot{\boldsymbol{J}}_\zeta(\boldsymbol{\sigma}_b,\boldsymbol{\zeta})\dot{\boldsymbol{\zeta}} + \boldsymbol{J}_\sigma(\boldsymbol{\sigma}_b,\boldsymbol{\zeta})\ddot{\boldsymbol{\sigma}}_b + \dot{\boldsymbol{J}}_\sigma(\boldsymbol{\sigma}_b,\boldsymbol{\zeta})\dot{\boldsymbol{\sigma}}_b\right), \quad (14)$$

where $\boldsymbol{J}_\zeta^\dagger = \boldsymbol{J}_\zeta{}^{\mathrm{T}}\left(\boldsymbol{J}_\zeta\boldsymbol{J}_\zeta{}^{\mathrm{T}}\right)^{-1}$ is a right pseudoinverse of $\boldsymbol{J}_\zeta$, $\boldsymbol{K}_v$ and $\boldsymbol{K}_p$ are symmetric positive definite gain matrices, $\boldsymbol{e}$ is the kinematic inversion error between the desired end-effector pose $\boldsymbol{x}_{e,d}$ and the actual pose $\boldsymbol{x}_e$ computed via the direct kinematics on the basis of $\boldsymbol{\zeta}$ and $\boldsymbol{\sigma}_b$. If the unit quaternions are used for the end-effector orientation, the error can be computed as (Chiaverini and Siciliano, 1999)

$$\boldsymbol{e} = \begin{bmatrix}\boldsymbol{e}_P \\ \boldsymbol{e}_O\end{bmatrix} = \begin{bmatrix}\boldsymbol{p}_{e,d} - \boldsymbol{p}_e(\boldsymbol{\sigma}_b,\boldsymbol{\zeta}) \\ \boldsymbol{R}_{e,d}\,\tilde{\boldsymbol{\epsilon}}(\boldsymbol{\sigma}_b,\boldsymbol{\zeta})\end{bmatrix}, \quad (15)$$

where $\tilde{\boldsymbol{\epsilon}}$ is the vectorial part of the unit quaternion extracted from the mutual orientation matrix $\boldsymbol{R}_{e,d}^T\boldsymbol{R}_e(\boldsymbol{\sigma}_b,\boldsymbol{\zeta})$. If $n+4 > 6$ the system is kinematically redundant and the redundant DOFs can be exploited to fulfill secondary tasks, otherwise, if no secondary tasks are required, the internal motions, i.e, motions of the structure that do not change the end-effector pose, must be stabilized via a suitable designed damping term to be projected onto the null space of $\boldsymbol{J}_\zeta$ (Hsu et al., 1988).

3.2 Motion Control

Once $\boldsymbol{\zeta}_r$ and its derivatives are computed by (14), they are fed to the motion control to achieve the desired motion. The proposed controller is an extension of that in Arleo et al. (2013), in turn, it is a hierarchical inner-outer loop control scheme: the outer loop is designed to track the vehicle reference position; then, by using the relation between the force vector $\boldsymbol{u}_f$ and the quadrotor attitude, a reference value for the roll and pitch angles is devised and fed to the attitude controller (inner loop). Finally, a controller for the arm joint positions is designed.

In order to globally linearize the closed-loop dynamics, the following adaptive control law can be considered

$$\boldsymbol{u} = \boldsymbol{M}(\boldsymbol{\xi})\boldsymbol{\alpha} + \boldsymbol{C}(\boldsymbol{\xi},\dot{\boldsymbol{\xi}})\dot{\boldsymbol{\xi}} + \boldsymbol{g}(\boldsymbol{\xi}) + \widehat{\boldsymbol{d}}(\boldsymbol{\xi},\dot{\boldsymbol{\xi}}), \quad (16)$$

where the auxiliary input $\boldsymbol{\alpha}$ can be partitioned according to (11) as $\boldsymbol{\alpha} = \left[\boldsymbol{\alpha}_p{}^{\mathrm{T}}\ \boldsymbol{\alpha}_\phi{}^{\mathrm{T}}\ \boldsymbol{\alpha}_q{}^{\mathrm{T}}\right]^{\mathrm{T}}$, with $\boldsymbol{\alpha}_\phi = [\alpha_\psi\ \alpha_\theta\ \alpha_\varphi]^{\mathrm{T}}$. The term $\hat{\boldsymbol{d}} = \left[\widehat{\boldsymbol{d}}_p^{\mathrm{T}}\ \widehat{\boldsymbol{d}}_\phi^{\mathrm{T}}\ \widehat{\boldsymbol{d}}_q^{\mathrm{T}}\right]^{\mathrm{T}}$ is an estimate of the disturbance $\boldsymbol{d}$ in (10).

The auxiliary controls $\boldsymbol{\alpha}_q$ and $\boldsymbol{\alpha}_p$ and α_ψ can be chosen as

$$\boldsymbol{\alpha}_q = \ddot{\boldsymbol{q}}_r + \boldsymbol{K}_{q,V}(\dot{\boldsymbol{q}}_r - \dot{\boldsymbol{q}}) + \boldsymbol{K}_{q,P}(\boldsymbol{q}_r - \boldsymbol{q}), \quad (17)$$

$$\boldsymbol{\alpha}_p = \ddot{\boldsymbol{p}}_r + \boldsymbol{K}_{p,V}(\dot{\boldsymbol{p}}_r - \dot{\boldsymbol{p}}) + \boldsymbol{K}_{p,P}(\boldsymbol{p}_r - \boldsymbol{p}), \quad (18)$$

$$\alpha_\psi = \ddot{\psi}_r + k_{\psi,V}(\dot{\psi}_r - \dot{\psi}) + k_{\psi,P}(\psi_r - \psi), \quad (19)$$

where $\boldsymbol{K}_{*,V}, \boldsymbol{K}_{*,P}$ $(* = \{q,p\})$ are symmetric positive definite matrices and $k_{\psi,V}$, $k_{\psi,P}$ are positive scalar gains.

Quadrotor position controller. On the basis of (16), the following expression of $\boldsymbol{u}_f$ can be derived

$$\boldsymbol{u}_f = \boldsymbol{M}_{pp}\boldsymbol{\alpha}_p + \boldsymbol{M}_{p\phi}\boldsymbol{\alpha}_\phi + \boldsymbol{M}_{pq}\boldsymbol{\alpha}_q + \boldsymbol{C}_p\dot{\boldsymbol{\xi}} + \boldsymbol{g}_p + \widehat{\boldsymbol{d}}_p. \quad (20)$$

This expression does not allow to compute $\boldsymbol{u}_f$, since it includes the control $\boldsymbol{\alpha}_\phi$, whose computation requires references values for roll and pitch angles, not available at this stage. To overcome this problem, let us replace the matrix $\boldsymbol{M}$ in (16) with the matrix $\overline{\boldsymbol{M}}$, obtained by setting to zero the second and third columns of $\boldsymbol{M}_{p\phi}$, namely $\overline{\boldsymbol{M}}_{p\phi} = [\,\boldsymbol{m}_{p\phi}\ \boldsymbol{0}_3\ \boldsymbol{0}_3\,]$. Thus, $\boldsymbol{u}_f$ can be computed as

$$\boldsymbol{u}_f = \boldsymbol{M}_{pp}\boldsymbol{\alpha}_p + \boldsymbol{m}_{p\phi}\alpha_\psi + \boldsymbol{M}_{pq}\boldsymbol{\alpha}_q + \boldsymbol{C}_p\dot{\boldsymbol{\xi}} + \boldsymbol{g}_p + \widehat{\boldsymbol{d}}_p. \quad (21)$$

It can be noted that, since the manipulator links are much lighter than the vehicle body, the elements of matrix $\boldsymbol{M}_{p\phi}$ are often negligible with respect to those of $\boldsymbol{M}_{pp}$ (Arleo et al., 2013). Therefore, in practice, $\boldsymbol{u}_f$ in (21) is very close to the ideal control input computed in (20).

In view of (11), $\boldsymbol{u}_f$ depends on the attitude of the quadrotor via the relation

$$\boldsymbol{u}_f = \boldsymbol{h}(f_z,\boldsymbol{\sigma}_b) \Rightarrow \begin{bmatrix}u_{f,x}\\ u_{f,y}\\ u_{f,z}\end{bmatrix} = \begin{bmatrix}(c_\psi s_\theta c_\varphi + s_\psi s_\varphi)\,f_z\\ (s_\psi s_\theta c_\varphi - c_\psi s_\varphi)\,f_z\\ c_\theta c_\varphi f_z\end{bmatrix}. \quad (22)$$

Therefore, the total thrust, f_z, and reference trajectories for the roll and pitch angles to be fed to the inner loop can be computed as

$$f_z = \|\boldsymbol{u}_f\|, \quad (23)$$

$$\theta_r = \arctan\left(\frac{u_{f,x}c_\psi + u_{f,y}s_\psi}{u_{f,z}}\right), \quad (24)$$

$$\varphi_r = \arcsin\left(\frac{u_{f,x}s_\psi - u_{f,y}c_\psi}{\|\boldsymbol{u}_f\|}\right). \quad (25)$$

Remark 1. It is worth noticing that (24)–(25) are not well defined if $\|\boldsymbol{u}_f\|$ vanishes, but from (22) it can happen only if $f_z = 0$, namely in presence of total thrust null. Moreover, they imply that both θ_r and ϕ_r are defined in $(-\pi/2\ \ \pi/2)$: this is a reasonable assumption for quadrotor vehicles.

Quadrotor attitude control. Once the reference value for roll and pitch angles have been computed, the control inputs α_θ and α_φ can be obtained via

$$\alpha_\theta = \ddot{\theta}_r + k_{\theta,V}(\dot{\theta}_r - \dot{\theta}) + k_{\theta,P}(\theta_r - \theta), \quad (26)$$

$$\alpha_\varphi = \ddot{\varphi}_r + k_{\varphi,V}(\dot{\varphi}_r - \dot{\varphi}) + k_{\varphi,P}(\varphi_r - \varphi), \quad (27)$$

where $k_{\theta,P}$, $k_{\theta,V}$, $k_{\varphi,P}$ and $k_{\varphi,V}$ are positive scalar gains. It is worth noticing that (26) and (27) require the knowledge of the time derivative of θ_r and φ_r, that can not be directly obtained by (22), but only via numerical differentiation.

Since in a practical scenario θ_r and φ_r are likely to be affected by noise, it can be realistic compute the reference velocities ($\dot{\theta}_r$ and $\dot{\varphi}_r$) by using suitable filters but their derivative can be very noisy, thus it is possible to modify (26) and (27) by adopting simple PD control laws as

$$\bar{\alpha}_\theta = k_{\theta,V}(\dot{\theta}_r - \dot{\theta}) + k_{\theta,P}(\theta_r - \theta) , \quad (28)$$

$$\bar{\alpha}_\varphi = k_{\varphi,V}(\dot{\varphi}_r - \dot{\varphi}) + k_{\varphi,P}(\varphi_r - \varphi) . \quad (29)$$

Finally, $\boldsymbol{u}_\mu$ can be computed as

$$\boldsymbol{u}_\mu = \boldsymbol{M}_{p\phi}{}^{\mathrm{T}}\boldsymbol{\alpha}_p + \boldsymbol{M}_{\phi\phi}\boldsymbol{\alpha}_\phi + \boldsymbol{M}_{\phi q}\boldsymbol{\alpha}_q + \boldsymbol{C}_\phi\dot{\boldsymbol{\xi}} + \boldsymbol{g}_\phi + \widehat{\boldsymbol{d}}_\phi, \quad (30)$$

and, from (11), the vehicle torques as

$$\boldsymbol{\mu}_b^b = \boldsymbol{R}_b^{\mathrm{T}}(\boldsymbol{\phi}_b)\boldsymbol{T}^{-\mathrm{T}}(\boldsymbol{\phi}_b)\boldsymbol{u}_\mu. \quad (31)$$

Computation of quadrotor inputs. Once f_z and $\boldsymbol{\mu}_b^b$ have been computed, the four actuation forces of the vehicle rotors can be easily obtained by inverting the (12).

Manipulator control. Finally, the torques acting on the manipulator joints can be computed as

$$\boldsymbol{u}_q = \boldsymbol{M}_{p\phi}^{\mathrm{T}}\boldsymbol{\alpha}_p + \boldsymbol{M}_{\phi q}^{\mathrm{T}}\boldsymbol{\alpha}_\phi + \boldsymbol{M}_{qq}\boldsymbol{\alpha}_q + \boldsymbol{C}_q\dot{\boldsymbol{\xi}} + \boldsymbol{g}_q + \widehat{\boldsymbol{d}}_q. \quad (32)$$

3.3 Uncertainties estimation

By considering the control law (21) in lieu of (20), and the input $\bar{\boldsymbol{\alpha}}_\phi = [\alpha_\psi, \bar{\alpha}_\theta, \bar{\alpha}_\varphi]^{\mathrm{T}}$ in lieu of $\boldsymbol{\alpha}_\phi$, the closed-loop dynamics is

$$\ddot{\boldsymbol{\xi}} = \boldsymbol{\alpha} - \Delta\boldsymbol{\alpha} - \boldsymbol{M}(\boldsymbol{\xi})^{-1}\left(\Delta\boldsymbol{M}\bar{\boldsymbol{\alpha}} + \boldsymbol{d} - \widehat{\boldsymbol{d}}\right), \quad (33)$$

where $\Delta\boldsymbol{M}(\boldsymbol{\xi}) = \boldsymbol{M}(\boldsymbol{\xi}) - \overline{\boldsymbol{M}}(\boldsymbol{\xi})$, and $\Delta\boldsymbol{\alpha} = \boldsymbol{\alpha} - \bar{\boldsymbol{\alpha}}$, with $\bar{\boldsymbol{\alpha}} = [\boldsymbol{\alpha}_p{}^{\mathrm{T}}\bar{\boldsymbol{\alpha}}_\phi{}^{\mathrm{T}}\boldsymbol{\alpha}_q{}^{\mathrm{T}}]^{\mathrm{T}}$.

Thus, the compensation term $\widehat{\boldsymbol{d}}$ has to take into account not only the modeling uncertainties, $\boldsymbol{d}$, but also the perturbation given by the practical implementation of the control law, namely the use of $\overline{\boldsymbol{M}}$ and $\bar{\boldsymbol{\alpha}}$ instead of $\boldsymbol{M}$ and $\boldsymbol{\alpha}$ in (16). To this aim, let us rearrange the (33) as

$$\ddot{\boldsymbol{\xi}} = \boldsymbol{\alpha} - \boldsymbol{\delta} + \widehat{\boldsymbol{\delta}} = \boldsymbol{\alpha} - \widetilde{\boldsymbol{\delta}}, \quad (34)$$

where

$$\boldsymbol{\delta} = \Delta\boldsymbol{\alpha} + \boldsymbol{M}(\boldsymbol{\xi})^{-1}(\Delta\boldsymbol{M}\bar{\alpha} + \boldsymbol{d}), \quad \widehat{\boldsymbol{\delta}} = \boldsymbol{M}(\boldsymbol{\xi})^{-1}\widehat{\boldsymbol{d}}.$$

A good approximations of the term $\boldsymbol{\delta}$ can be obtained by resorting to a parametric model, i.e.,

$$\boldsymbol{\delta} = \boldsymbol{\Lambda}(\boldsymbol{\xi})\boldsymbol{\chi} + \boldsymbol{\varsigma}, \quad (35)$$

where $\boldsymbol{\Lambda}$ is a regressor matrix, $\boldsymbol{\chi}$ is a vector of constant parameters and $\boldsymbol{\varsigma}$ is the interpolation error. Of course, not all uncertainties can be rigorously characterized by a linear-in-the-parameters structure, however, this modeling assumption is not too restrictive, since it has been demonstrated that it is valid for a wide class of functions (Caccavale et al., 2013). The elements of the regressor matrix can be chosen as Radial Basis Functions (RBFs)

$$\lambda_{i,h}(\boldsymbol{\xi}) = \exp\left(-\frac{||\boldsymbol{\xi} - \boldsymbol{c}_{i,h}||}{2\sigma^2}\right), \quad (36)$$

where $\boldsymbol{c}_{i,h}$ and σ are the centroids and the width of the function, respectively. According to the Universal Interpolation Theorem (Haykin, 1999), under mild assumptions, any continuous function can be approximated by a RBF-newtork with a bounded interpolation error $\boldsymbol{\varsigma}$.

Therefore, $\boldsymbol{\delta}$ can be estimated via the estimate $\widehat{\boldsymbol{\chi}}$ of $\boldsymbol{\chi}$ obtained by designing the following update law

$$\dot{\widehat{\boldsymbol{\chi}}} = \frac{1}{\beta}\boldsymbol{\Lambda}^{\mathrm{T}}\boldsymbol{B}^{\mathrm{T}}\boldsymbol{Q}\begin{bmatrix}\widetilde{\boldsymbol{\xi}}\\ \dot{\widetilde{\boldsymbol{\xi}}}\end{bmatrix}, \quad (37)$$

where β is a positive scalar gain, $\boldsymbol{Q}$ is a symmetric and positive definite matrix, $\boldsymbol{B} = [\boldsymbol{O}_{6+n} \;\; \boldsymbol{I}_{6+n}]^{\mathrm{T}}$ and $\widetilde{\boldsymbol{\xi}} = \boldsymbol{\xi}_r - \boldsymbol{\xi}$.

4. STABILITY ANALYSIS

To prove the stability of the closed-loop system, let us consider the convergence to zero of both the kinematic control outer loop and the motion control inner loop.

4.1 Inner loop

By considering (33), the following dynamics for the inner loop error $\widetilde{\boldsymbol{\xi}}$ can be derived

$$\ddot{\widetilde{\boldsymbol{\xi}}} = -\boldsymbol{\Omega}_V\dot{\widetilde{\boldsymbol{\xi}}} - \boldsymbol{\Omega}_P\widetilde{\boldsymbol{\xi}} + \widetilde{\boldsymbol{\delta}}, \quad (38)$$

where (for $* = V, P$)

$$\boldsymbol{\Omega}_* = \begin{bmatrix}-\boldsymbol{K}_{p,*} & \boldsymbol{O}_3 & \boldsymbol{O}_3\\ \boldsymbol{O}_3 & -\boldsymbol{K}_{\Phi,*} & \boldsymbol{O}_3\\ \boldsymbol{O}_n & \boldsymbol{O}_n & -\boldsymbol{K}_{q,*}\end{bmatrix},$$

Let us rearrange the (38) in the state space form by considering $\boldsymbol{z} = [\boldsymbol{z}_1{}^{\mathrm{T}}\;\boldsymbol{z}_2{}^{\mathrm{T}}]^{\mathrm{T}} = [\widetilde{\boldsymbol{\xi}}^{\mathrm{T}}\;\dot{\widetilde{\boldsymbol{\xi}}}^{\mathrm{T}}]^{\mathrm{T}}$ and by assuming $\boldsymbol{\varsigma} = \boldsymbol{0}$

$$\dot{\boldsymbol{z}} = \boldsymbol{\Omega}\boldsymbol{z} + \boldsymbol{B}\widetilde{\boldsymbol{\delta}} = \boldsymbol{\Omega}\boldsymbol{z} + \boldsymbol{B}\boldsymbol{\Lambda}\widetilde{\boldsymbol{\chi}}, \quad (39)$$

where $\widetilde{\boldsymbol{\chi}} = \boldsymbol{\chi} - \widehat{\boldsymbol{\chi}}$ and $\boldsymbol{\Omega} = \begin{bmatrix}\boldsymbol{O}_{6+n} & \boldsymbol{I}_{6+n}\\ -\boldsymbol{\Omega}_V & -\boldsymbol{\Omega}_P\end{bmatrix}$. In order to analyze the stability of the system (39), the following Lyapunov candidate function could be considered

$$V_i = \frac{1}{2}\boldsymbol{z}^{\mathrm{T}}\boldsymbol{Q}\boldsymbol{z} + \frac{\beta}{2}\widetilde{\boldsymbol{\chi}}^{\mathrm{T}}\widetilde{\boldsymbol{\chi}}. \quad (40)$$

The time derivative of V_i yields

$$\dot{V}_i = -\boldsymbol{z}^{\mathrm{T}}\boldsymbol{P}_z\boldsymbol{z} + \boldsymbol{z}^{\mathrm{T}}\boldsymbol{Q}\boldsymbol{B}\boldsymbol{\Lambda}\widetilde{\boldsymbol{\chi}} + \beta\dot{\widetilde{\boldsymbol{\chi}}}^{\mathrm{T}}\widetilde{\boldsymbol{\chi}}, \quad (41)$$

where $\boldsymbol{P}_z = -(\boldsymbol{Q}\boldsymbol{\Omega} + \boldsymbol{\Omega}^{\mathrm{T}}\boldsymbol{Q})$ is the symmetric and positive definite solution of the Lyapunov equation that always exists since $\boldsymbol{\Omega}$ is Hurwitz. By assuming the parameter $\boldsymbol{\chi}$ constant or, at least, slowly-varying, and by considering the update law (37), $\dot{V}_i$ can be rewritten as

$$\dot{V}_i = -\boldsymbol{z}^{\mathrm{T}}\boldsymbol{P}_z\boldsymbol{z} + \boldsymbol{z}^{\mathrm{T}}\boldsymbol{Q}\boldsymbol{B}\boldsymbol{\Lambda}\widetilde{\boldsymbol{\chi}} - \beta\dot{\widehat{\boldsymbol{\chi}}}^{\mathrm{T}}\widetilde{\boldsymbol{\chi}} = -\boldsymbol{z}^{\mathrm{T}}\boldsymbol{P}_z\boldsymbol{z}. \quad (42)$$

Since $\boldsymbol{P}_z$ is positive definite, $\dot{V}_i$ is negative semi-definite; this guarantees the boundedness of $\boldsymbol{z}$ and $\widetilde{\boldsymbol{\chi}}$. By invoking the Barbalat's lemma (Khalil, 1996), it can be recognized that $\dot{V}_i \to 0$, which implies the global asymptotic convergence to $\boldsymbol{0}$ of $\boldsymbol{z}$ as $t \to \infty$, while, as usual in direct adaptive control (Aström and Wittenmark, 1995), $\widetilde{\boldsymbol{\chi}}$ is only guaranteed to be uniformly bounded, i.e., $\|\widetilde{\boldsymbol{\chi}}| \leq \overline{\chi}$.

Moreover, if the persistency of excitation (PE) condition is fulfilled (Aström and Wittenmark, 1995) both $\boldsymbol{z}$ and $\widetilde{\boldsymbol{\chi}}$ are exponentially convergent to $\boldsymbol{0}$.

In the presence of bounded estimation error $\boldsymbol{\varsigma}$ the PE ensures that both $\boldsymbol{z}$ and $\widetilde{\boldsymbol{\chi}}$ are bounded, while if PE cannot be met, to ensure the boundedness of $\widetilde{\boldsymbol{\chi}}$ the update law (37) can be modified by adopting the so-called *projection operator* (Aström and Wittenmark, 1995).

4.2 Kinematic control outer loop

Under the assumption of perfect acceleration tracking (i.e. $\ddot{\boldsymbol{\zeta}} = \ddot{\boldsymbol{\zeta}}_r$), by substituting (14) in (13), the following holds

$$\dot{\boldsymbol{v}}_{e,d} - \dot{\boldsymbol{v}}_e = -\boldsymbol{K}_v\left(\boldsymbol{v}_{e,d} - \boldsymbol{v}_e\right) - \boldsymbol{K}_p\boldsymbol{e}. \tag{43}$$

Let us consider, the following inverse kinematics error

$$\boldsymbol{\varepsilon} = \begin{bmatrix} \boldsymbol{\varepsilon}_P \\ \boldsymbol{\varepsilon}_O \end{bmatrix}, \quad \boldsymbol{\varepsilon}_P = \begin{bmatrix} \boldsymbol{e}_P \\ \dot{\boldsymbol{e}}_P \end{bmatrix}, \quad \boldsymbol{\varepsilon}_O = \begin{bmatrix} \boldsymbol{e}_O \\ \widetilde{\boldsymbol{\omega}}_e \end{bmatrix}, \tag{44}$$

where $\boldsymbol{e}_P$ and $\boldsymbol{e}_O$ are defined in (15), while $\widetilde{\boldsymbol{\omega}}_e = \boldsymbol{\omega}_{e,d} - \boldsymbol{\omega}_e$. To prove the symptotic stability of the equilibrium point $\boldsymbol{\varepsilon} = \boldsymbol{0}$ let us consider the following candidate Lyapunov function (Chiaverini and Siciliano, 1999)

$$V_o = (\eta_d - \eta)^2 + (\boldsymbol{\epsilon}_d - \boldsymbol{\epsilon})^{\mathrm{T}}(\boldsymbol{\epsilon}_d - \boldsymbol{\epsilon}) + \widetilde{\boldsymbol{\omega}}_e^{\mathrm{T}}\widetilde{\boldsymbol{\omega}}_e + \boldsymbol{\varepsilon}_P^{\mathrm{T}}\boldsymbol{Q}_P\boldsymbol{\varepsilon}_P, \tag{45}$$

where η (η_d) and $\boldsymbol{\epsilon}$ ($\boldsymbol{\epsilon}_d$) are the scalar part and the vector part of the unit quaternion representing the end-effector (desired) orientation and $\boldsymbol{Q}_P$ is a symmetric and positive matrix. The time derivative of V_o is given by

$$\begin{aligned} \dot{V}_o = & -\boldsymbol{e}_O^{\mathrm{T}}\boldsymbol{K}_{p,O}\boldsymbol{e}_O - 2\widetilde{\boldsymbol{\omega}}_e^{\mathrm{T}}\boldsymbol{K}_{v,O}\widetilde{\boldsymbol{\omega}}_e - 2\widetilde{\boldsymbol{\omega}}_e^{\mathrm{T}}\boldsymbol{K}_{p,O}\boldsymbol{e}_O \\ & + \boldsymbol{\varepsilon}_P^{\mathrm{T}}\left(\boldsymbol{Q}_P\boldsymbol{A}_P + \boldsymbol{A}_P^{\mathrm{T}}\boldsymbol{Q}_P\right)\boldsymbol{\varepsilon}_P, \end{aligned} \tag{46}$$

where $\boldsymbol{K}_{*,O}$ $(* = v, p)$ is the matrix including the last three row of matrix $\boldsymbol{K}_*$, and

$$\boldsymbol{A}_P = \begin{bmatrix} \boldsymbol{O}_3 & \boldsymbol{I}_3 \\ -\boldsymbol{K}_{p,P} & -\boldsymbol{K}_{v,P} \end{bmatrix}.$$

with $\boldsymbol{K}_{*,P}$ $(* = v, p)$ the matrix including the first three row of matrix $\boldsymbol{K}_*$. Since $\boldsymbol{A}_P$ is Hurwitz, always exists a matrix $\boldsymbol{P}_P$, symmetric and positive definite, solution of the Lyapunov equation in (46), hence

$$\begin{aligned} \dot{V}_o \leq & -\lambda_m(\boldsymbol{K}_{p,O})\|\boldsymbol{e}_O\|^2 - 2\lambda_m(\boldsymbol{K}_{v,O})\|\widetilde{\boldsymbol{\omega}}_e\|^2 \\ & + 2\lambda_M(\boldsymbol{K}_{p,O})\|\widetilde{\boldsymbol{\omega}}_e\|\|\boldsymbol{e}_O\| - \lambda_m(\boldsymbol{P}_P)\|\boldsymbol{e}_P\|^2 \\ \leq & -\begin{bmatrix} \|\boldsymbol{e}_O\| \\ \|\widetilde{\boldsymbol{\omega}}_e\| \end{bmatrix}^{\mathrm{T}} \boldsymbol{\Xi} \begin{bmatrix} \|\boldsymbol{e}_O\| \\ \|\widetilde{\boldsymbol{\omega}}_e\| \end{bmatrix} - \lambda_m(\boldsymbol{P}_P)\|\boldsymbol{e}_P\|^2, \end{aligned} \tag{47}$$

with

$$\boldsymbol{\Xi} = \begin{bmatrix} \lambda_m(\boldsymbol{K}_{p,O}) & -\lambda_M(\boldsymbol{K}_{p,O}) \\ -\lambda_M(\boldsymbol{K}_{p,O}) & 2\lambda_m(\boldsymbol{K}_{v,O}) \end{bmatrix},$$

and $\lambda_m(\cdot)$ and $\lambda_M(\cdot)$ representing the minumum and maximum eigenvalue of a matrix. If the following holds

$$\lambda_m(\boldsymbol{K}_{v,o}) > \frac{\lambda_M^2(\boldsymbol{K}_{p,o})}{2\lambda_m(\boldsymbol{K}_{p,o})}, \tag{48}$$

matrix $\boldsymbol{\Xi}$ is positive definite, therefore $\dot{V}_o$ can be upper bounded as

$$\dot{V}_o \leq -\lambda_m(\boldsymbol{\Xi})\|\boldsymbol{\varepsilon}_O\|^2 - \lambda_m(\boldsymbol{P}_P)\|\boldsymbol{\varepsilon}_P\|^2 \leq -\lambda_\varepsilon\|\boldsymbol{\varepsilon}\|^2, \tag{49}$$

where $\lambda_\varepsilon = \min\{\lambda_m(\boldsymbol{\Xi}), \lambda_m(\boldsymbol{P}_P)\}$.
Thus, since $\dot{V}_o$ is negative definite the error $\boldsymbol{\varepsilon}$ is asymptotically convergent to zero.

4.3 Two-loops dynamics

Under the assumption of perfect acceleration tracking, for the two-loops dynamics, by considering the following Lyapunov candidate function

$$V = V_o(\boldsymbol{\varepsilon}) + V_i(\boldsymbol{z}), \tag{50}$$

it is straightforward derived from (42) and (47) that $\dot{V}$ is negative definite and both $\boldsymbol{\varepsilon}$ and $\boldsymbol{z}$ are globally asymptotically convergent to zero. Moreover the convergence is exponential in the absence of interpolation error ($\boldsymbol{\varsigma} = \boldsymbol{0}$) and in the presence of PE for the regressor $\boldsymbol{\Lambda}$.

However, in practice the inner loop cannot guarantee instantaneous perfect tracking of the desired joint acceleration, therefore by considering the error $\ddot{\tilde{\boldsymbol{\zeta}}} = \ddot{\boldsymbol{\zeta}}_r - \ddot{\boldsymbol{\zeta}}$, the (43) becomes

$$\dot{\boldsymbol{v}}_{e,d} - \dot{\boldsymbol{v}}_e = -\boldsymbol{K}_v\left(\boldsymbol{v}_{e,d} - \boldsymbol{v}_e\right) - \boldsymbol{K}_p\boldsymbol{e} + \boldsymbol{J}_\zeta\ddot{\tilde{\boldsymbol{\zeta}}}. \tag{51}$$

The perturbation term $\boldsymbol{J}_\zeta\ddot{\tilde{\boldsymbol{\zeta}}}$ can be upper bounded as

$$\|\boldsymbol{J}_\zeta\ddot{\tilde{\boldsymbol{\zeta}}}\| \leq \|\boldsymbol{J}_\zeta\|\|\ddot{\tilde{\boldsymbol{\zeta}}}\| \leq \|\boldsymbol{J}_\zeta\|\|\dot{\boldsymbol{z}}_2\| \leq \|\boldsymbol{J}_\zeta\|\left(\|\boldsymbol{\Omega}\|\|\boldsymbol{z}\| + \|\widetilde{\boldsymbol{\delta}}\|\right).$$

Since, in the presence of PE and in the absence of interpolation error, it can be viewed as a vanishing perturbation, by resorting to Lemma 9.1 in Khalil (1996) it can be stated that the equilibrium point $\{\boldsymbol{\varepsilon} = \boldsymbol{0}, \boldsymbol{z} = \boldsymbol{0}\}$, is again exponentially stable. On the contrary, if the PE condition cannot be met and/or bounded interpolation error ($\|\boldsymbol{\varsigma}\| \leq \overline{\varsigma}$) is present, $\boldsymbol{J}_\zeta\ddot{\tilde{\boldsymbol{\zeta}}}$ can be seen as a bounded non-vanishing perturbation and the errors $\boldsymbol{\varepsilon}$ and $\boldsymbol{z}$ are only bounded (Lemma 9.2 in Khalil (1996)).

5. SIMULATION RESULTS

The proposed algorithm has been tested in simulation by using the Matlab/SimMechanics© environment and by considering a quadrotor equipped with a 5-DOF robotic manipulator with all revolute joints. In the simulation model, to set both the dynamic parameters (mass and inertia moments) and the Denavit-Hartenberg parameters for the robotic arm, the values used in Arleo et al. (2013) have been considered. In order to simulate the model uncertainties, $\boldsymbol{d}$, only a nominal estimate of the inertia matrix has been considered available for the controller, namely its elements are assumed to be equal to 0.9 times their true values.

In order to simulate a realistic scenario, it has been assumed that only vehicle position, orientation and Euler angles' rate, as well as, manipulator joint position measurements are available. Linear velocities, joint velocities and angular accelerations measurements for roll and pitch angles, $\ddot{\boldsymbol{\sigma}}_b$, have been obtained via a first-order filter with a time constant of 0.03 s, from the available positions and velocities measurements. All the measured data have been considered available at a frequency rate of 250 Hz. Moreover, a normally distributed measurement noise has been added to the available signals: in detail for vehicle position the noise has mean of 10^{-3} m and standard deviation of $5 \cdot 10^{-3}$ m, for vehicle orientation the mean is 10^{-3} rad and the standard deviation is 10^{-3} rad, for the attitude rates the mean is $5 \cdot 10^{-3}$ rad/s and the standard deviation is $5 \cdot 10^{-3}$ rad/s and for the joint position the mean is 10^{-4} rad and the standard deviation is $5 10^{-4}$ rad. The controller parameters are summarized in Table 1.

The end-effector is tasked to follow the 3D trajectory reported in Fig. 3. At the end of the path an hovering phase of 5 s is commanded. Moreover, a rotation of $\pi/5$ rad along roll, pitch and yaw axes is required as well.

Table 1. Controller parameters

Gain	Value	Gain	Value
$\boldsymbol{K}_{p,P}$, $\boldsymbol{K}_{p,V}$	$12 \cdot \boldsymbol{I}_3$, $5 \cdot \boldsymbol{I}_3$	$\boldsymbol{K}_{q,P}$, $\boldsymbol{K}_{q,V}$	$140\boldsymbol{I}_5$, $20\boldsymbol{I}_5$
$k_{\psi,P}$, $k_{\psi,V}$	8, 3	$k_{\theta,P}$, $k_{\theta,V}$	2, 1
$k_{\varphi,P}$, $k_{\varphi,V}$	2, 1	$\boldsymbol{K}_p$, $\boldsymbol{K}_v$	$7.5\boldsymbol{I}_6$, $0.6\boldsymbol{I}_6$
β	4	–	–

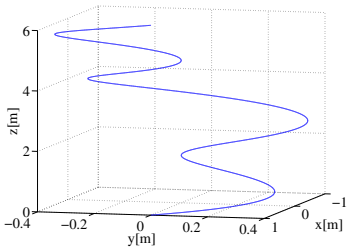

Fig. 3. 3D desired trajectory of the end-effector.

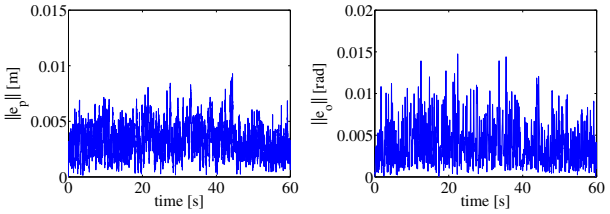

(a) position error (b) orientation error

Fig. 4. End-effector pose error norm.

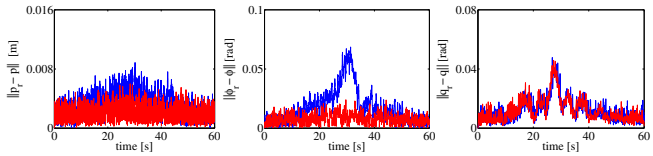

(a) vehicle position (b) vehicle orientation (c) joint position

Fig. 5. Norm of the motion control errors, with (blue line) and without (red line) the adaptive term

Fig. 4(a) and Fig. 4(b) depict the norm of the end-effector pose error between the desired and the actual trajectory: it can be seen that the controller guarantees good tracking capabilities since the maximum errors are comparable with the measurement noise. The motion control errors are shown in Fig. 5: it represents the norm of the position and orientation errors relative to the UAV (Fig. 5(a)–5(b)), as well as the norm of joint errors Fig. 5(c). More in details, the figures show a comparison between the error obtained by set to zero the adaptive term, $\widehat{\boldsymbol{\delta}}$, and that obtained by using the adaptive term: it can be recognized that the adaptive term improves the attitude and the position control of the quadrotor, while the manipulator joint controller is almost insensitive to it. This is due both to the presence of $\overline{\boldsymbol{M}}$ and $\bar{\boldsymbol{\alpha}}$ that affect only the vehicle dynamics, and to the fact that the link are very lightweight and the uncertainties on matrix $\boldsymbol{M}$ do not compromise the joint controller performance.

REFERENCES

Antonelli, G., Arrichiello, F., Chiaverini, S., and Robuffo Giordano, P. (2013). Adaptive trajectory tracking for quadrotor mavs in presence of parameter uncertainties and external disturbances. In *Proc. of IEEE/ASME Int. Conf. on Advanced Intelligent Mechatronics*, 1337–1342.

Arleo, G., Caccavale, F., Muscio, G., and Pierri, F. (2013). Control of quadrotor aerial vehicles equipped with a robotic arm. In *Proc. of 21th Mediterranean Conference on Control and Automation*, 1174–1180.

Aström, K. and Wittenmark, B. (1995). *Adaptive control (2nd ed.)*. Addison-Wesley.

Bouabdallah, S. and Siegwart, R. (2005). Backstepping and sliding-mode techniques applied to an indoor micro quadrotor. In *Proc. of the IEEE Int. Conf. on Robotics and Automation (ICRA)*, 2259–2264.

Caccavale, F., Chiaverini, S., and Siciliano, B. (1997). Second-order kinematic control of robot manipulators with jacobian damped least-squares inverse: Theory and experiments. *IEEE/ASME Trans. on Mechatronics*, 2, 188–194.

Caccavale, F., Marino, A., Muscio, G., and Pierri, F. (2013). Discrete-time framework for fault diagnosis in robotic manipulators. *IEEE Trans. on Control Systems Technology,*, 21(5), 1858–1873.

Chiaverini, S. and Siciliano, B. (1999). The unit quaternion: A useful tool for inverse kinematics of robot manipulators. *Systems Analysis Model. Simul.*, 35, 45–60.

Haykin, S. (1999). *Neural Networks: A Comprehensive Foundation*. Prentice Hall, Upper Saddle River, NJ.

Hoffmann, G., Huang, H., Waslander, S., and Tomlin, C. (2007). Quadrotor helicopter flight dynamics and control: Theory and experiment. In *Proc. of the AIAA Guidance, Navigation, and Control Conf. and Exhibit*.

Hsu, P., Hauser, J., and Sastry, S. (1988). Dynamic control of redundant manipulators. In *Proc. of IEEE Int. Conf. on Robotics and Automation*, 183–187.

Kendoul, F., Fantoni, I., and Lozano, R. (2008). Asymptotic stability of hierarchical inner-outer loop-based flight controllers. In *Proc. of the 17th IFAC World Congress*, 1741–1746.

Khalil, H. (1996). *Nonlinear Systems (2nd ed.)*. Prentice Hall, Upper Saddle River, NJ.

Kim, H. and Shim, D. (2003). A flight control system for aerial robots: Algorithms and experiments. *Control Engineering Practice*, 11(2), 1389–1400.

Kondak, K., Krieger, K., Albu-Schaeffer, A., Schwarzbach, M., Laiacker, M., Maza, I., Rodriguez-Castano, A., and Ollero, A. (2013). Closed-loop behavior of an autonomous helicopter equipped with a robotic arm for aerial manipulation tasks. *International Journal of Advanced Robotic Systems*, 10(145), 1–9.

Lippiello, V. and Ruggiero, F. (2012). Cartesian impedance control of uav with a robotic arm. In *Proc. of 10th Int. IFAC Symp. on Robot Control*, 704–709.

Maza, I., Kondak, K., Bernard, M., and Ollero, A. (2010). Multi-UAV cooperation and control for load transportation and deployment. *Journal of Intelligent and Robotic Systems*, 57, 417–449.

Nonami, K., Kendoul, F., Suzuki, S., and Wang, W. (2010). *Atonomous Flying Robots, Unmanned Aerial Vehicles and Micro Aerial Vehicles*. Springer, London.

Palunko, I. and Fierro, R. (2011). Adaptive control of a quadrotor with dynamic changes in the center of gravity. In *Proc. of the 18th IFAC World Congress*, 2626–2631.

Pounds, P., Bersak, D., and Dollar, A. (2011). Vision based mav navigation in unknown and unstructured environments. In *Proc. of IEEE Int. Conf. on Robotics and Automation (ICRA)*, 2491–2498.

Siciliano, B., Sciavicco, L., Villani, L., and Oriolo, G. (2009). *Robotics – Modelling, Planning and Control*. Springer, London, UK.

Spica, R., Franchi, A., Oriolo, G., Blthoff, H., and Robuffo Giordano, P. (2012). Aerial grasping of a moving target with a quadrotor UAV. In *Proc. of IEEE/RSJ Int. Conf. on Intelligent Robots and Systems (IROS)*, 4985–4992.